Journal Name

ARTICLE

Nanosized LiFePO$_4$-decorated emulsion-templated carbon foam for 3D micro batteries: A study of structure and electrochemical performance

Habtom D. Asfaw,[a] Matthew R. Roberts[a], Cheuk-Wai Tai[b], Reza Younesi[a], Mario Valvo[a], Leif Nyholm[a] and Kristina Edström[a*]

In this article, we report a novel 3D composite cathode fabricated from LiFePO$_4$ nanoparticles deposited conformally on emulsion-templated carbon foam by a sol-gel method. The carbon foam is synthesized via a facile and scalable method which involves the carbonization of a high internal phase emulsion (polyHIPE) polymer template. Various techniques (XRD, SEM, TEM and electrochemical methods) are used to fully characterize the porous electrode and confirm the distribution and morphology of the cathode active material. The major benefits of the carbon foam used in our work are closely connected with its high surface area and the plenty of space suitable for sequential coating with battery components. After coating with a cathode material (LiFePO$_4$ nanoparticles), the 3D electrode presents a hierarchically structured electrode in which a porous layer of the cathode material is deposited on the rigid and bicontinuous carbon foam. The composite electrodes exhibit impressive cyclability and rate performance at different current densities affirming their importance as viable power sources in miniature devices. Footprint area capacities of 1.72 mAhcm^{-2} at 0.1 mAcm^{-2} (lowest rate) and 1.1 mAhcm^{-2} at 6 mAcm^{-2} (highest rate) are obtained when the cells are cycled in the range 2.8 to 4.0 v vs. lithium.

Introduction

Current efforts in microelectronics are geared towards the fabrication of integrated and self-sufficient devices in which a computing processor, communicators, sensors and on-board power sources are packed into a volume of 1-5 mm^3.[1, 2] In such applications where space is limited, power sources that are sufficiently small, yet able to provide as much energy as required at the desired rates, should be employed. Notable examples are microscale batteries and supercapacitors.[3] Both 2D and 3D electrode configurations are being studied. Unlike thin and thick film microbatteries, 3D electrodes are tailored to applications which seek to utilize an increased amount of active materials at high rates.[4] In this context, a variety of electrode architectures has been proposed including an array of electrodes,[5, 6] 3D ordered macroporous (3DOM) electrodes,[7, 8] perforated and trenched electrodes[9, 10] and so on.

One type of feasible electrodes considered for the realization of microbatteries is a porous carbon. Porous carbon electrodes have long been investigated as promising candidates for use in various electrochemical systems such as batteries,[11, 12] supercapacitors,[13] electrocatalysis,[14] capacitive deionization,[15] fuel cells[16] and hydrogen storage.[17] Particularly, their use in 3D batteries has attracted much interest in recent years. This is partly related to the desirable attributes that carbon imparts such as its good electrical conductivity, versatility, abundance, cost and light weight. An ideal porous carbon electrode is required to be (a) fully networked to support electron flow throughout the entirety of the electrode architecture (b) non-tortuous to facilitate ion transport with minimum ohmic drop (c) mechanically stiff to avoid detachment of the active materials during cycling (d) electrochemically stable in the working voltage window and (e) able to provide a high surface area available for coating with active materials and an electrolyte. This permits operation of the 3D battery at sustained high rates with little or no side reactions and capacity fading.

In recent years, there has been an increasing trend in the synthesis of LiFePO$_4$ particles embedded in porous carbon.[18-21] The sole purpose of the carbon scaffold is to facilitate electron transfer across the current collector and active material interface and allow percolation of electrolyte by virtue of its porosity. Even though this kind of electrode fabrication led to effective utilization of active materials and dramatic improvement in high rate capacities, it still necessitated the usage of additional conductive matrix and a binder. One strategy for avoiding these additives is to deposit the active material directly onto the surfaces of the networked porous carbon which will serve as a support and a current collector. To achieve this, the porous carbon is desired to be mechanically sturdy to withstand pressure and have pore dimensions suitable for the layer-by-layer deposition of all the battery components. In this regard, carbon foams can be cited as best examples. Notably, electrodeposition of MnO$_2$ on RVC (reticulated vitreous carbon) foam[22] and a thick layer of polyaniline on emulsion-templated carbon foam[23] was successfully used to demonstrate the benefits and suitability of carbon foams for microbattery applications. Remarkable cyclability and rate capabilities were noted for these electrodes.
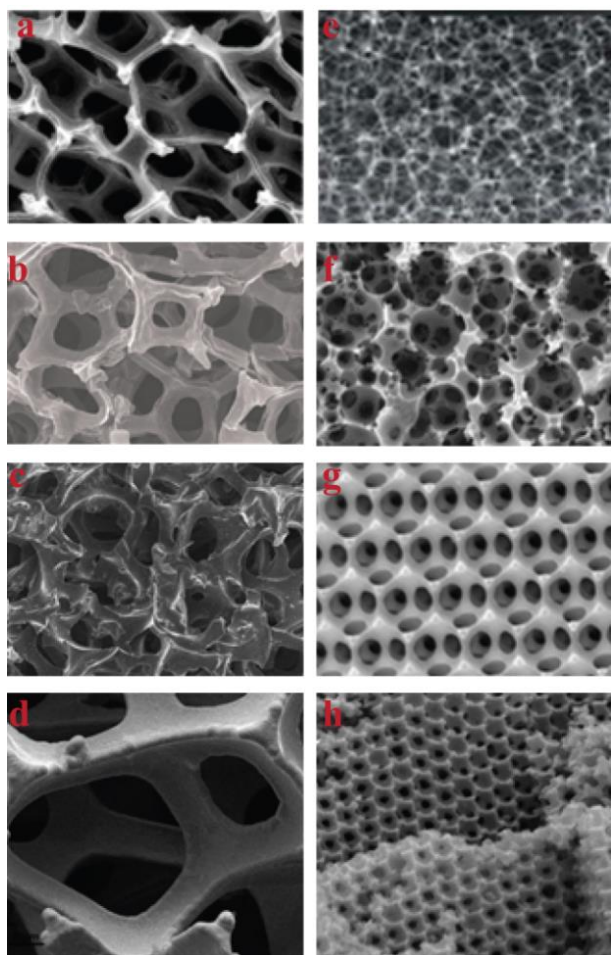
Figure 1: Different types of carbon foams are listed in order of decreasing void (macropore) sizes. Comparison is made based on the number of voids each material contains along a millimetre (vpm): (a) graphite carbon foam 2 vpm,[24] Reprinted with permission from Ref 24. Copyright (2012) American Chemical Society (b) graphene carbon foam 3 vpm.[25] Reproduced from Ref. 25 with permission from The Royal Society of Chemistry. (c) reticulated vitreous carbon from Goodfellow 4 vpm, (d) graphene carbon foam 13 vpm, from ACS materials, (e) melamine-derived carbon foam 20 vpm,[26] Reproduced from Ref. 26 with permission from The Royal Society of Chemistry. (f) emulsion-templated carbon foam 50 vpm, (g) 3DOM carbon foam > 2000 vpm[27]. Adapted from Ref. 27 with permission from The Royal Society of Chemistry, and (h) Colloidal silica and polymer-templated 3DOM carbon 6000 vpm.[28] Reprinted with permission from Ref 28. Copyright 2010 American Chemical Society

Several examples of carbon foams are given in Figure 1. Here, a unit termed vpm (voids per millimeter) is used to express the number of voids (macropores) each material contains along a millimeter. Manual measurements are done on the scanning electron micrographs to estimate the mean diameters of the macropores which comprise the carbon foams. A polyHIPE-derived carbon foam, which is shown in Figure 1 (f) and is the focus of this paper, possesses macropores measuring around 20 μm on average, which can be given as 50 vpm. A structure of this type is more ideal than 3DOMs in that it presents a plenty of room into which layers of active materials and an electrolyte can be deposited to fabricate freestanding 3D thin or thick film microbatteries. Since the carbon foam possesses reasonably good electrical conductivity, a layer of polymer electrolyte can be electrodeposited on top of the active materials. This is a key attribute of conductive electrode structures required for the realization of fully integrated 3D batteries. Previously, we have shown how such materials are suitable for use in micro-

structured batteries as they present ideal length scale for construction of a fully integrated 3D battery system. The polyHIPE-derived carbon foam serves as a current collector which affords enough free space to accommodate an electrode/electrolyte/electrode/current collector stack within the pores. Until now, we have demonstrated that such highly porous materials can be conformally coated via electrodeposition (with some thinning of the deposited layer towards the foam center) of polyaniline. The polyaniline coated carbon foams delivered excellent electrochemical performance with the state of the art areal capacity. However, polyaniline (and other conducting polymers) is not conventionally used in lithium ion batteries due to its low volumetric capacities, large voltage range and issues with self-discharge.[29]

In this work, we have adopted a sol-gel coating methodology to apply a conformal layer of $LiFePO_4$ on the surface of polyHIPE –derived carbon foam. $LiFePO_4$, particularly in its nano-sized form, has become a topical material for a wide range of applications and it is noted for its remarkable cyclability and rate performance.[30-36] It has a competitive gravimetric capacity (170 mA h g^{-1}), volumetric capacity (612 mA h cm^{-3}), a flat discharge plateau operating at 3.45 V (within most solvent stability windows) and is well known to offer high stability and excellent safety. These advantages make the development of 3D microstructured cathodes based on this material particularly interesting for the further development of fully integrated systems. It is hoped that this highly conductive current collector cathode architecture will provide an excellent substrate for the subsequent deposition of electrolyte/electrode structures.

Experimental

Synthesis of polyHIPE-derived carbon foams

Generally, HIPE can be prepared by a thorough mixing of a continuous phase and a much greater proportion of internal phase in the presence of a suitable surfactant.[37, 38] The continuous phase undergoes polymerization and cross-linking while the droplet phase evaporates leaving behind a highly porous and networked polymer. This polymer is subsequently functionalized, as required, and pyrolyzed to prepare porous carbon foam. First, a high internal phase emulsion was prepared by mixing an oil phase containing 6 mL Styrene, 3 mL DVB, 1 mL VBC and 3 g Span80 as a surfactant and a droplet-forming aqueous solution of $CaCl_2.2H_2O$ and $K_2S_2O_8$ initiator. The emulsion was stirred vigorously for 5 minutes before being transferred to a PTFE mold. Then it was polymerized at 65 °C for 48 hours in an oven. The polymers were chopped to pieces and washed with ethanol and water. Afterwards, the clean pieces were sulfonated overnight with concentrated sulfuric acid to render them stable towards high temperature treatment. The sulfonated polymers were washed with water and dried at 100 °C. Then, they were carbonized in a tube furnace (Heraeus® Tube Furnace) in Ar atmosphere at 900 °C.

Coating in $LiFePO_4$

Thin pieces of as-prepared polyHIPE-derived carbon foams were immersed in a sol-gel precursor of $LiFePO_4$ which consisted of 0.2 M $FeSO_4.7H_2O$, 0.2M $NH_4H_2PO_4$, 0.4 M citric acid, 0.2M lithium acetate in a 9:1 mixture of distilled water and methanol. The solution containing the carbon foams was evacuated in a vacuum chamber to drive out air from and to force the solution into the mesopores. The pieces were taken out and dried at 70 °C overnight. Then they were dried under vacuum at 120 °C overnight. The dried carbon foams were heated in a tube furnace (Heraeus® Tube Furnace) up to 700 °C at a rate of 1 °C/min in Ar atmosphere for 8 hours.

Characterization

X-ray Diffraction(XRD):- A piece of LiFePO$_4$-coated carbon foam was crushed to a powder and dispersed in acetone. The dispersion was then cast on a flat silicon sample holder and mounted on the diffractometer (Siemens D5000 using copper K$_\alpha$ radiation source, λ= 1.5418) to collect X-ray diffraction pattern of the synthesized LiFePO$_4$.

Scanning Electron Microscopy (SEM):- Scanning electron micrographs of the external and cross-section of coated carbon electrodes were taken using SEM/EDS – Zeiss 1550 instrument (15 kV is used) and a secondary electron detector.

Transmission Electron Microscopy (TEM):- Transmission electron microscopy analysis (TEM and STEM) of finely powdered sample, which were dispersed in acetone and sonicated for several minutes, was done using a JEOL JEM-2100F microscope operated at 200 kV and equipped with a Gatan Ultrascan 1000 CCD camera and JEOL annular dark-field (ADF) detector.

Electrochemical testing

All samples were dried under vacuum at 120°C overnight prior to use. Pouch cells were assembled in an Ar-filled glove box using coated carbon foams (footprint areas ranging from 0.12 to 0.20 cm^{-2}, ~400 μm in thickness) and lithium foil anodes spaced in between by glass fiber separators soaked in electrolyte (1M LiPF$_6$ in 1:1 EC:DEC). Cyclability and rate performance of the half-cells were evaluated by cyclic voltammetry and galvanostatically in the voltage range 2.8 to 4.0 V versus lithium using Biologic VMP2. Similar tests were performed on pristine carbon foam in the same voltage range versus lithium in order to verify the electrochemical stability of the carbon and the electrolyte used. All capacities are normalized to the footprint area of the electrodes used. The amount of LiFePO$_4$ contained in the electrode was calculated as follows. A piece of the coated carbon foam was dried at 60 °C for two days and its mass was recorded. Then, it was immersed in a concentrated solution of HCl and digested at 50 °C for several hours to completely dissolve the LiFePO$_4$ coating. The carbon foam was recovered and washed with acidified distilled water and with ethanol repeatedly. It was finally dried at 60 °C for two days and weighed to determine the mass loss which was assigned to LiFePO$_4$. The gravimetric capacity was calculated based on the mass of LiFePO$_4$.

XPS

The samples (pristine and cycled carbon foams) were washed by dimethyl carbonate (DMC) in an Argon-filled glove box prior to XPS measurements, and then were transferred to the XPS analysis chamber using an air-tight argon filled module to avoid contaminations from air. The XPS measurements were carried out using a commercial PHI 5500 spectrometer, using monochromatic Al Kα radiation (1487 eV) and an electron emission angle of 45°. All the XPS spectra were energy-calibrated by the hydrocarbon peak positioned at the binding energy of 285.0 eV.

Results and discussion

This section consists of three parts. The first part deals with the synthesis and the coating of the carbon foam and characterization of the composite electrode using x-ray diffraction to confirm the synthesis of LiFePO$_4$ in the desired phase and purity. In the second section, electron microscopy techniques are used to shed light on the particle morphology, size distribution and consistency of the coating on the 3D carbon networks. Following that is a description of a thorough electrochemical testing wherein galvanostatic and voltammetric techniques are employed to evaluate the performance of the 3D cathode at various current densities. In addition, a brief discussion will be made on the stability of the electrolyte in contact with the carbon electrode in the voltage window used

(detailed description is included in the supplementary information).

Synthesis of carbon foam and coating in LiFePO$_4$

The salient feature of the carbon foam derived from high internal phase emulsion polymers is its highly networked structure built from open-celled cages (10-50 μm in diameter) interconnected by windows (1-20 μm). In Figure 2 (a), photos of the polymer and carbon foams are shown along with a 3D schematic picture of the microstructures of the carbon foam. Based on the preparation method and the functionalization of the polymer precursors, significant amount of porosity can be introduced into the walls of the carbon foams. Typically, sulfonation is used to introduce crosslinking in the polymers and render them stable towards high temperatures during carbonization. Apart from this, sulfonation activates the surface of the polymers and contributes to the formation of mesopores and micropores in the walls of the carbon foams after pyrolysis. Consequently, the carbon foam presents a high specific surface area (estimated by nitrogen gas sorption), $A_{BET} = 433$ m^{2}g^{-1}. A detailed description of the synthesis and characterization of polyHIPE-derived carbons is provided in earlier works by Wang et al. and our group.[23]
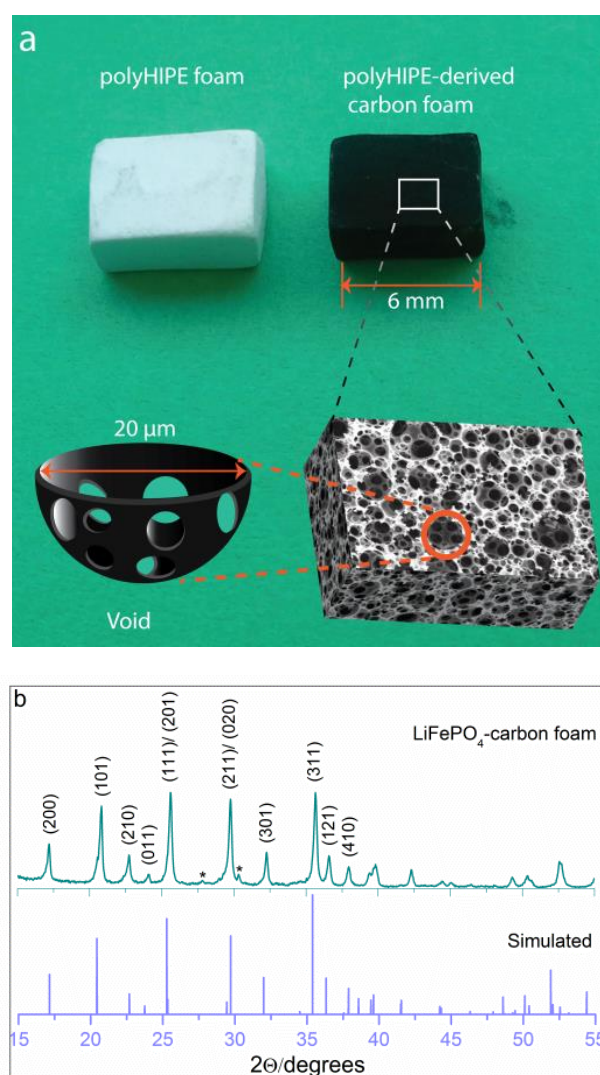
Figure 2: (a) Polymer and carbon foams: photos of polyHIPE polymer template and carbon foam (top) and 3D visualization of the carbon foam (bottom). (b) The XRD pattern of the synthesized LiFePO$_4$ (impurity peaks are indicated by *)

To take advantage of the high surface area available, we have tried to coat the carbon foams with a layer of LiFePO$_4$ via a sol-gel method. Commonly, a sol-gel solution used for the synthesis of LiFePO$_4$ co

nsists of precursor salts and citric acid dissolved in water. Since the s urface of pristine carbon exhibits a certain degree of hydrophobicity towards water, depositing a conformal coating of precursor materials of LiFePO$_4$ from aqueous solutions is challenging. To enhance the w ettability of carbon by water, different strategies have been employe d such as functionalization of the carbon surface. In this work, we us ed a mixture of water and methanol to reduce the surface tension of water and increase the wettability of the carbon foam. This simple str ategy facilitates the infiltration of the sol-gel solution into the porous carbon structure and ensures a secure adhesion of the coating to the c arbon after synthesis. The x-ray diffraction (XRD) pattern for the sy nthesized material is given in Figure 2(b). All the peaks indicated in the XRD pattern (except some extremely weaker impurity peaks) ca n be indexed to the Pnma space group and correspond to the olivine phase of LiFePO$_4$.

Electron microscopy characterization

Electron microscopy techniques are used to gain insight into the nature of the coating on the carbon foam such as its thickness, the morphology and distribution of the active material in the coating, and the overall topography of the 3D porous electrode. To accomplish these, scanning electron microscopy, scanning transmission electron microscopy and electron dispersive spectroscopy are used.
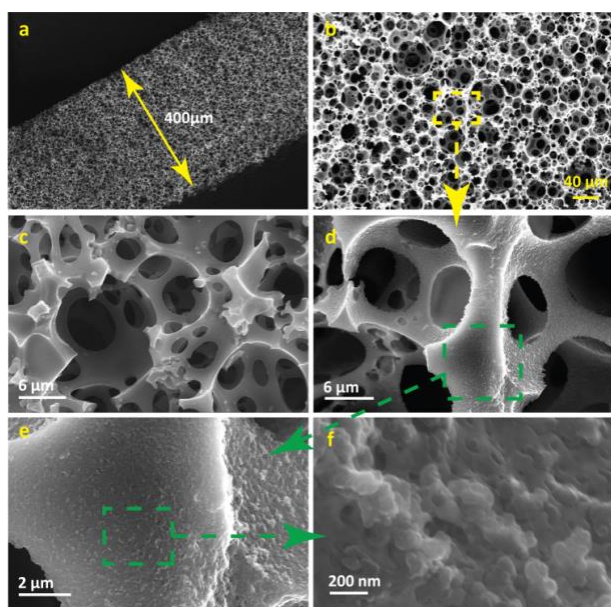
Figure 3: A slice of the carbon foam (a), approximately 400 μm in thickness, is coated in a layer of LiFePO$_4$ nanoparticles by a sol-gel method. Micrographs in Figures a and b represent the coated carbon foam at lower magnifications. Comparing the SEMs of the bare (c) and coated (d) carbon foam show that a layer of LiFePO4 is deposited on the carbon foam. Images e and f offer better insight into the nature of the coating.

The microstructures of the open-celled carbon foams (400 μm in thickness) before and after coating are shown in the scanning electron micrographs (SEM) in Figure 3. The pristine (uncoated) carbon foam is shown in (c) whereas (a), (b) and (d)-(f) represent the coated carbon foam. Comparing the two sets of SEMs confirms the success of the coating. As evidenced by the micrographs, a more or less conformal deposition of LiFePO$_4$ nanoparticles is achieved on the walls of the porous carbon foam. As a result, a hierarchically structured composite electrode is obtained, i.e., a porous LiFePO$_4$-carbon layer is coated onto the walls of the interconnectivities of the carbon foam. This can be seen more clearly in the micrograph given in Figure S1. However, the measurement of the thickness indicated in the micrograph is not accurate as the edge of the layer is slanted.

The synthesis of LiFePO$_4$ via sol-gel route has previously been reported to give crystalline particles embedded in a highly porous layer of carbon.[39] The porosity is believed to facilitate electrolyte percolation thereby enhancing mass transport during battery operation. In interest of facilitating mass transfer across the electrode and accommodating the remaining components of the 3D battery, it is very crucial that no blocking of the open-celled framework should occur anywhere in the electrode after depositing the LiFePO$_4$ layer. In this regard, one can see that the coating on our electrode is mostly on the surface of the carbon framework and there is no blocking of the voids and the windows of the carbon foam.
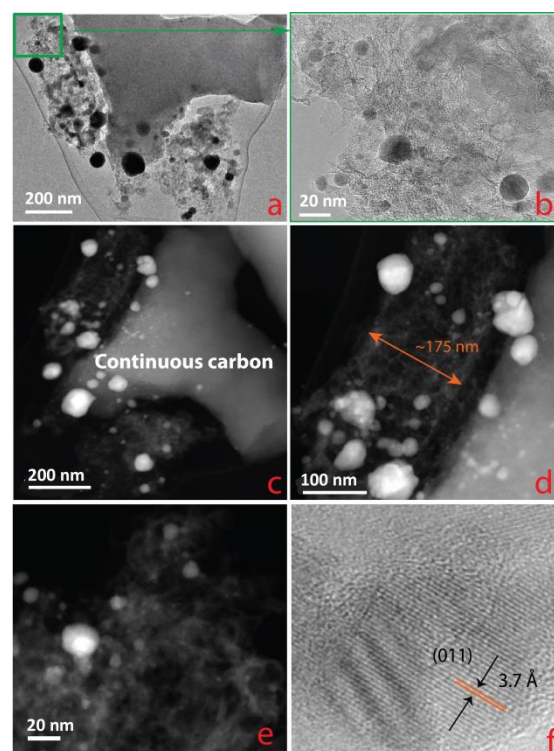
Figure 4: Transmission electron microscopy characterization of LiFe PO$_4$ nanoparticles synthesized in polyHIPE-derived carbon foams: (a) TEM-BF images: dark spots represent LiFePO$_4$ nanoparticles (b) a magnified image of a selected area from (a). (c), (d) and (e) are HA ADF-STEM images of LiFePO4-coated carbon foam in which LiFe PO$_4$ particles appear bright. Image f is a high resolution TEM of the crystallites.

Further details about the distribution and morphology of the cathode material come from transmission electron microscopy (TEM) and Sc anning transmission electron microscopy (STEM) data given in Figu re 4. In the bright field TEM (TEM-BF) images, in Figure 4 (a) and (b), the LiFePO$_4$ particles are shown as circular dark areas scattered o ver a bright background. A close-up image of a selected part of the i mage reveals that even smaller particles can be obtained. A better co ntrast and morphology of the nanoparticles and an accentuated topog raphy of the porous electrode can clearly be seen in the high angle an nular dark field (HAADF-STEM) images in Figure 4 (c)-(e). Since c ontrast in the HAADF-STEM of a given compound is dependent on t he atomic number of the comprising elements, we can safely conclud e that the bright (white) particles which are scattered on a relatively darker background (carbon) represent the LiFePO$_4$ nanoparticles. In agreement with the SEM data illustrated above, the STEM images sh ow that the nanoparticles are trapped in a porous carbon matrix whic h forms an intimate coating on the continuous interconnects of the ca rbon foam. Figure 4 (d) shows a LiFePO$_4$-carbon layer measuring ro ughly about 175 nm rests on the carbon foam. A schematic represent ation given in Figure 5 visualizes the hierarchical structure of the ele ctrode.
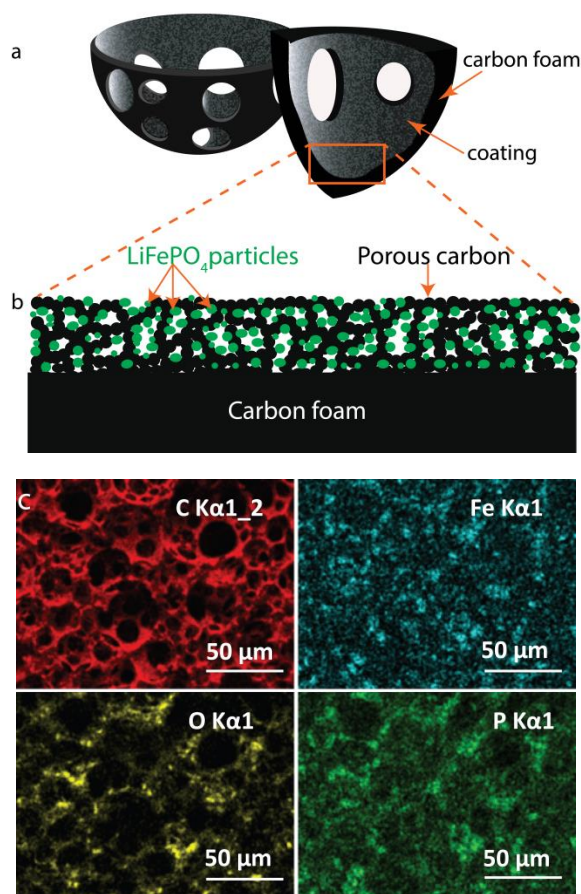
Figure 5: Schematic of a porous LiFePO4-carbon layer deposited on a continuous carbon foam. The open-celled void (a) which can be taken as the building block of the carbon foam is covered with a porous layer of LiFePO4 particles trapped in carbon residues (b). EDX maps show elemental distribution on the coated carbon foam (c).

As mentioned above obliquely, the composite electrode consists of two types of carbons: the continuous framework of the carbon foam (Figure 4 (c)) and the porous carbon matrix originating from the pyrolysis of the citric acid (Figure 4 (e)). The relatively brighter contrast of the continuous carbon may be associated to its thickness. Most of the nanosized LiFePO4 particles are found embedded in the porous carbon layer which is in turn deposited on the surface of the continuous carbon foam, as can be seen in Figures 4 (c) and 5. This aids in keeping the particles together in the coating and wiring them to the continuous electrode. In short, this composite electrode features a thin cathode layer fixed on a bicontinuous carbon electrode by a carbon aerogel which provides a reticulated pathway for electron transport. Apart from this, the thin porous cathode layer guarantees fast charge and mass transfer and thus a greatly enhanced power performance can be obtained. In the EDX maps displayed in Figure 2(b), one can observe the elemental distribution across the porous electrode, hinting at the uniform distribution of LiFePO4. Here, it is worth noting that the carbon observed in the EDX map comes from the porous carbon on which the coating is deposited and the carbon residues resulting from the pyrolysis of citric acid which is used as a chelating ligand in the sol-gel precursor solution. These data show that LiFePO4 has been successfully deposited on the bicontinuous carbon. Another important feature of the cathode is related to the size distribution of the particles. On the basis of the SEM and STEM data, it can be concluded that there exists a wide distribution of particle sizes of LiFePO4, with the majority of the particles (above 80%) being below 70 nanometers in size, as shown in Figure S2. The effect of the small size of the

particles is manifest in their electrochemical behavior as described in the following section.

Electrochemical testing

Substrate testing

Results from the electrochemical stability test of the bare carbon foam versus lithium are given in the supplementary information (Figure S3 and S4). We assume that the current response from the pristine porous carbon is the total sum of the contributions due to capacitive effects (double layer charging) as a consequence of the large surface area and parasitic oxidative reactions involving the electrolyte in the presence of traces of moisture or other contaminants that are adsorbed on carbon and the Al contact. After few cycles, the surface of the electrode is passivated and parasitic reactions cease to occur, as observed in Figure S3.[40, 41] However, the effect of the parasitic and capacitive current on the LiFePO4-coated carbon foam is barely visible, since its contribution is insignificant as compared to faradaic processes pertaining to the active material. The contribution of the carbon substrate to the overall capacity of the composite cathode amounts to ~ 1.2 % and ~ 0.8 % at current densities of ~ 0.1 mAcm^{-2} and 6 mAcm^{-2}, respectively (see Figure S4).

LiFePO4-coated carbon foam

In the preceding sections, evidence for the distribution, morphology and 3D structure of LiFePO4-coated carbon foam is successfully presented. The stability of the carbon foam in the working voltage window is also investigated. For the remainder of this section, we will focus on the electrochemical characterization of LiFePO4-coated carbon foam and its use as a cathode in 3D microbatteries. LiFePO4 is one of the most extensively investigated materials in lithium ion batteries and volumes of references are available on its synthesis, crystallographic structure, insertion mechanism, electrochemical performance, thermal stability and cycle life.[30, 32, 34, 36, 42-45]
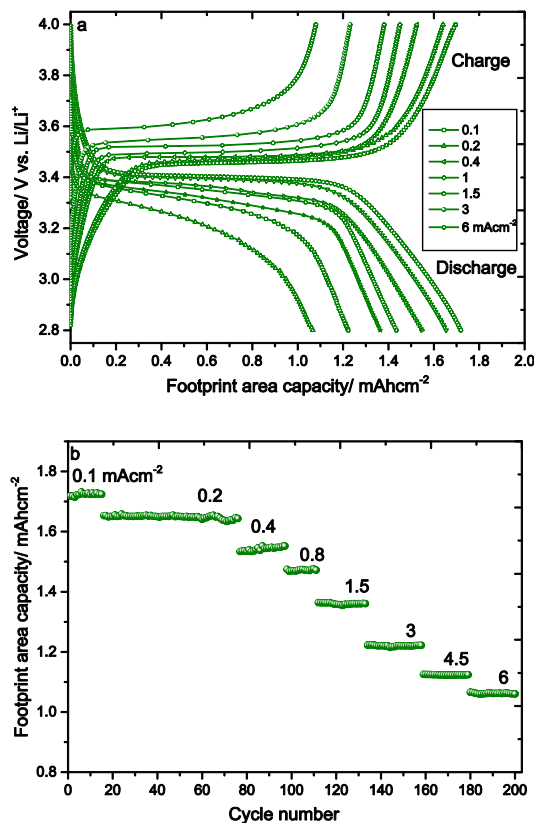
Figure 6: (a) The charge/discharge voltage profiles of LiFePO4-carbon foam at different current densities in the voltage range from 2.8 to 4.0 V vs. Li (b) rate performance at different current densities.

The overall charge-discharge characteristics of LiFePO$_4$-coated carbon foam at different current densities are shown in Figure 6a and S5. It can be noted that the discharge occurs with slightly sloping voltage profiles centered on 3.45 V vs. lithium, typical for nanosized LiFePO$_4$.[44, 46] The sloping in the voltage profiles is believed to stem from the formation of size-driven solid solutions of lithium rich and lithium deficient LiFePO$_4$ and is more pronounced at higher current densities as reported previously.[20, 47-49] Another noticeable feature of the voltage profiles is the tailing observed at the end of the flat regions of the charge and discharge profiles. In addition, there is a monotonic shift in redox potentials and concurrent decrease in capacity which scale directly with increasing current densities, especially for those higher than 0.2 mAcm^{-2} (see also Figure S5).

In Figure 6b, the rate performance corresponding to the different current densities is shown. The areal capacities obtained at current densities of 0.1, 0.2, 0.4 and 6 mAcm^{-2} are 1.72, 1.65, 1.55 and 1.07 mAh

cm^{-2}, respectively. A simple procedure, as detailed in the preceding section, is employed to quantify the amount of LiFePO$_4$ in the electrode. Accordingly, the amount of the active material is around 1.7 mg per 2.9 mg of carbon foam (which amounts to 37% of the total mass of the electrode) and constitutes a volumetric loading of 158 mg cm^{-3}. The gravimetric capacity at 0.2 mAcm^{-2} (~ 0.1 C-rate) is calculated to be approximately 157 mAhg^{-1} which corresponds to 92% of the theoretical capacity of LiFePO$_4$. Clearly, the electrode performs remarkably well at all rates in terms of both areal capacity and coulombic efficiency. The latter exceeds 99.5 % and almost 60% of the slow rate capacity is accessible at a current density 60 times higher. Table 1 in the supplementary information presents a summary of literature reports on different electrode materials suggested for use in microbatteries. In comparison, the performance of LiFePO$_4$-coated carbon foam compares remarkably well with those of the electrodes for which the highest footprint area capacities are reported in the literature.
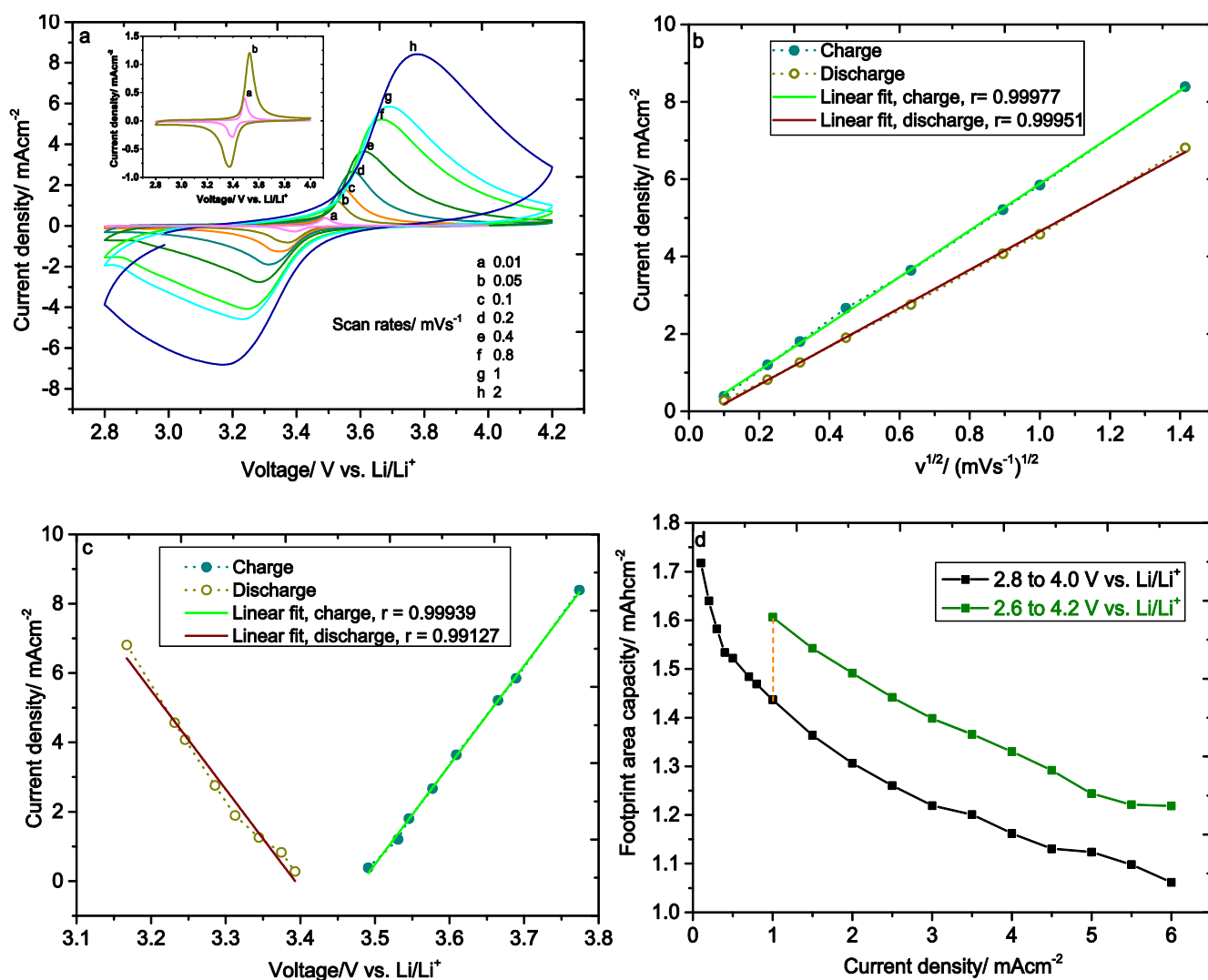
Figure 7: The decrease in the capacity observed at higher current rates is IR drop-controlled. (a) Cyclic voltammograms of LiFePO$_4$-coated carbon foam at different scan rates. (b) Linear dependence of peak current densities (absolute values) on the square root values of scan rates indicate that insertion/deinsertion of lithium ions in LiFePO$_4$ particles is diffusion-controlled. r stands for the correlation coefficient of linearity. (c) Plots of the absolute value of peak current density as a function of peak potential. (d) Discharge footprint area capacity as a function of the applied current density. Note the influence of the cut-off voltage on the ultimate capacity values.

Whilst the performance of this material is excellent, the source of the high rate capacity loss ought to be clarified. In order to understand the causes of capacity decrease with increasing current, we carried out cyclic voltammetric analysis in which the evolution of peak potential is monitored as the scan rate is increased progressively. One can see readily that there exists a noticeable difference between the cathodic

and anodic branches of each cyclic voltammogram in Figure 7 (a). The anodic peaks are relatively sharper and have higher peak current densities unlike their cathodic counter parts which are broader and show lower peak current densities. Despite the difference in the peak currents, the amounts of charge (integrated areas under the curves) passed over a certain period of time during charging and discharging are

nearly equal ($q_{discharge}/q_{charge} \approx 0.99$ in this case) as reported in previous works.[50, 51] Plots of charge and discharge peak current densities against square roots of scan rates, as shown in Figure 7 (b), portray the linear dependence of current density on the square root of scan rate. This behavior has been widely reported in other similar works and indicates that the electrochemical activity of LiFePO$_4$ is diffusion-controlled. Moreover, in all the CVs current exhibits, at the beginning of oxidation and reduction, a linear dependence on potential because of the internal cell resistance. In Figure 7 (c) and Figure S6, the nature of the correlation between current density and peak potential (E$_p$) is investigated. Apparently, the peak potential varies more linearly than logarithmically with the current density showing that the electrode processes are IR-controlled. For a porous electrode flooded with liquid electrolyte, ohmic losses are ascribed to the resistances of the solid matrix and the pore electrolyte.[52] Resistivity of the porous carbon is inherently resultant from the presence of thin and long pore interconnectivities and tortuous pores which impede ion transport in the pore electrolyte.[7] The internal resistance can be deduced from the IR drops observed at the beginning of the charge and discharge galvanostatic curves. A linear plot of IR drop versus current density is given in Figure S7. Accordingly, the resistance is 53 and 46 ohms for charge and discharge, respectively.

Extending the operating voltage window by 0.2 V (Figure 7 d), which should allow for a greater degree of reaction to take place, results in commensurate increments in areal capacities. However, the capacities obtained are still less than the slow rate capacity hinting at the possibility that other factors might be implicated in the capacity loss observed at higher cycling rates. Plausible explanations can be made on the basis of the facility of Li$^+$ ions diffusion in the solid active materials and the pore electrolyte. In the light of the CV results, the electrochemical cycling of LiFePO$_4$ entails the solid-state diffusion of Li$^+$ ions in/out of the active material and its rate determines the overall performance of the cell. In the higher scan rate (>0.8 mV s^{-1}) voltammograms in Figure 7a, it can be noted that the current appears to be tending towards a diffusion controlled situation suggesting that the reaction is not complete within the potential window of this experiment. The thickness of the coating on the carbon struts is 200 nm and is, as explained above, composed of LiFePO$_4$ particles surrounded by carbon residues. Given that the pore electrolyte in the carbon foam contains a large excess of lithium ions as compared to those required for a complete discharge of the available active material, bulk supply of the lithium ions from the electrolyte should not be an issue. Taking an average size of the LiFePO$_4$ particles (L) to be 40 nm (see Figure S2) and the apparent solid-state diffusion coefficient (D) ranging from 10^{-12} - 10^{-14} cm^{2}s^{-1},[50, 53-56] the time constant for 1D diffusion is of the order of

$$\tau \approx \frac{L^2}{2D} \approx 10 \ to \ 10^3 \ s.$$

The references given above explain the variation of the diffusivity of Li$^+$ ions with particle size, concentration of defects and the state of charge (SOC) of the active materials. Hence, all the lithium ions in a particle are not extracted/ inserted at the same rate of diffusion. At high charge/discharge rates the rate of diffusion will be insufficient to support the current imposed and hence the full capacity of the material cannot be attained as observed in Figure 6. For instance, the time taken for discharge at a current density of 6 mAcm^{-2} is roughly 11 minutes, which is not long enough to allow for the complete discharge of the FePO$_4$ particles. Another possible source of capacity loss can be explained somewhat by the geometry of the carbon foams. As explained at the beginning of the discussion section, the carbon foam is built from open voids of different sizes interconnected by windows. There is no uniformity in the pore interconnectivities and the pore size distribution in the electrode. We suppose that this will result in inhomogeneous current density distribution as seen previously from modelling[57] of trench microbattery and thus non-uniform rate of reaction arises in the entire electrode. Such inhomogeneous current densities cause local depletion of the pore electrolyte ions in certain regions of the electrode and limit the available capacity at higher rates. In brief, we suggest that these inhomogeneous current densities result in regions deficient in lithium ions and suppress the activity of the FePO$_4$ leading to incomplete discharge at higher rates.[47]

To summarize, we observe the 3D electrode provides excellent cyclability and rate performance which compare favorably well with the best values reported in other works. We believe that the capacity loss observed at higher current densities can be attributed to IR drop, diffusion limitations in the solid active materials and inhomogeneous current densities which in turn lead to incomplete utilization of the active materials as the electrode process ends prematurely owing to local electrolyte ion depletion.

Conclusions

In this article we have demonstrated the successful coating of a poly HIPE-derived carbon foam in LiFePO$_4$ nanoparticles by a sol-gel method and its potential use for 3D microbattery applications. The carbon foam used in this work has a high specific surface area, a well-interconnected structure and ideal macropore diameters, which make it a promising 3D electrode architecture for microbattery applications. Electron microscopy characterizations reveal that a hierarchically porous composite electrode is achieved. A porous layer of carbon residues in which the LiFePO$_4$ nanoparticles are embedded is in intimate contact with the networked carbon foam. When cycled in the range from 2.8 to 4.0 V vs. lithium, the composite electrode exhibits a noteworthy cyclability and rate performance at different current densities. Footprint area capacities of 1.72 mAhcm^{-2} at 0.1 mAcm^{-2} (lowest rate) and 1.1 mAhcm^{-2} at 6 mAcm^{-2} (highest rate) are obtained. It is our considered opinion that this type of structures can be used successfully to manufacture an integrated 3D electrode for microbatteries to be used as power sources in tiny devices. Another novelty value in this approach pertains to the feasibility of using the carbon foam current collector for a wide selection of active materials. The carbon foams can be used with almost all cathodes (LiCoO$_2$, Li$_2$FeSiO$_4$, MnO$_2$ etc.) and some high-voltage negative active materials such as TiO$_2$ and Li$_4$Ti$_5$O$_{12}$.

Acknowledgements

Notes and references

[a] Ångström Advanced Battery Centre (ÅABC), Department of Chemistry, Ångström Laboratory, Uppsala University, Box 538, SE-75121, Uppsala, SWEDEN

[b] Department of Materials and Environmental Chemistry, Arrhenius Laboratory, Stockholm University, S-10691, Stockholm, SWEDEN

[*] Corresponding author: kristina.edstrom@kemi.uu.se

1.   K. Edström, D. Brandell, T. Gustafsson and L. Nyholm, *Electrochem. Soc. Interface*, 2011, 20, 41-46.

2.   J. W. Long, B. Dunn, D. R. Rolison and H. S. White, *Chem. Rev.*, 2004, 104, 4463-4492.

3.   M. Beidaghi and Y. Gogotsi, *Energy Environ. Sci.*, 2014, 7, 867-884.

4.   M. Roberts, P. Johns, J. Owen, D. Brandell, K. Edstrom, G. El Enany, C. Guery, D. Golodnitsky, M. Lacey, C. Lecoeur, H. Mazor, E. Peled, E. Perre, M. M. Shaijumon, P. Simon and P.-L. Taberna, *J. Mater. Chem.*, 2011, 21, 9876-9890.

5.   P. L. Taberna, S. Mitra, P. Poizot, P. Simon and J. M. Tarascon, *Nature Mater.*, 2006, 5, 567-573.

6.   E. Perre, L. Nyholm, T. Gustafsson, P.-L. Taberna, P. Simon and K. Edström, *Electrochem. Commun.*, 2008, 10, 1467-1470.

7.   J. S. Sakamoto and B. Dunn, *J. Mater. Chem.*, 2002, 12, 2859-2861.

8.   H. P. James, Z. Hui Gang, C. Jiung, V. B. Paul and P. K. William, *Nat. Commun.*, 2013, 4, 1732-1732.

9.   P. H. L. Notten, F. Roozeboom, R. A. H. Niessen and L. Baggetto, *Adv. Mater.*, 2007, 19, 4564-4567.

10.   M. Nathan, D. Golodnitsky, V. Yufit, E. Strauss, T. Ripenbein, I. Shechtman, S. Menkin and E. Peled, J. *Microelectromech. S.*, 2005, 14, 879-885.

11.   G. He, S. Evers, X. Liang, M. Cuisinier, A. Garsuch and L. F. Nazar, *ACS Nano*, 2013, DOI: 10.1021/nn404439r.

12.   J. Yang, J. Wang, X. Li, D. Wang, J. Liu, G. Liang, M. Gauthier, Y. Li, D. Geng, R. Li and X. Sun, *J. Mater. Chem.*, 2012, 22, 7537-7543.

13.   Y. Gogotsi, A. Nikitin, H. Ye, W. Zhou, J. E. Fischer, B. Yi, H. C. Foley and M. W. Barsoum, *Nature Mater.*, 2003, 2, 591-594.

14.   A. Dorjgotov, J. Ok, Y. Jeon, S.-H. Yoon and Y. Shul, *J. Solid State Electrochem.*, 2013, 17, 2567-2577.

15.   S. Porada, L. Borchardt, M. Oschatz, M. Bryjak, J. S. Atchison, K. J. Keesman, S. Kaskel, P. M. Biesheuvel and V. Presser, *Energy Environ. Sci.*, 2013, 6, 3700-3712.

16.   S. Shrestha, S. Ashegi, J. Timbro and W. E. Mustain, *ECS Transactions*, 2013, 50, 1287-1299.

17.   S. J. Yang, T. Kim, J. H. Im, Y. S. Kim, K. Lee, H. Jung and C. R. Park, *Chem. Mater.*, 2012, 24, 464-470.

18.   C. M. Doherty, R. A. Caruso, B. M. Smarsly, P. Adelhelm and C. J. Drummond, *Chem. Mater.*, 2009, 21, 5300-5306.

19.   H. Ni, J. Liu and L.-Z. Fan, *Nanoscale*, 2013, 5, 2164-2168.

20.   J. Zhao, J. He, J. Zhou, Y. Guo, T. Wang, S. Wu, X. Ding, R. Huang and H. Xue, *J. Phys.Chem. C*, 2011, 115, 2888-2894.

21.   R. Dominko, M. Bele, J.-M. Goupil, M. Gaberscek, D. Hanzel, I. Arcon and J. Jamnik, *Chem. Mater.*, 2007, 19, 2960-2969.

22.   P. Johns, M. Roberts and J. Owen, *J. Mater. Chem.*, 2011, 21, 10153-10159.

23.   H. D. Asfaw, M. Roberts, R. Younesi and K. Edstrom, *J. Mater. Chem. A*, 2013, 1, 13750-13758.

24.   H. Ji, L. Zhang, M. T. Pettes, H. Li, S. Chen, L. Shi, R. Piner and R. S. Ruoff, *Nano Lett.*, 2012, 12, 2446-2451.

25.   D. A. C. Brownson, L. C. S. Figueiredo-Filho, X. Ji, M. Gomez-Mingot, J. Iniesta, O. Fatibello-Filho, D. K. Kampouris and C. E. Banks, *J. Mater. Chem. A*, 2013, 1, 5962-5972.

26.   S. Chen, G. He, H. Hu, S. Jin, Y. Zhou, Y. He, S. He, F. Zhao and H. Hou, *Energy Environ. Sci.*, 2013, 6, 2435-2439.

27.   Z. Wang, E. R. Kiesel and A. Stein, *J. Mater. Chem.*, 2008, 18, 2194-2200.

28.   S. Zhang, L. Chen, S. Zhou, D. Zhao and L. Wu, *Chem. Mater.*, 2010, 22, 3433-3440.

29.   P. Novák, K. Müller, K. S. V. Santhanam and O. Haas, *Chem. Rev.*, 1997, 97, 207-282.

30.   L.-X. Yuan, Z.-H. Wang, W.-X. Zhang, X.-L. Hu, J.-T. Chen, Y.-H. Huang and J. B. Goodenough, *Energy Environ. Sci.*, 2011, 4, 269-284.

31.   J. Wang and X. Sun, *Energy Environ. Sci.*, 2012, 5, 5163-5185.

32.   R. Malik, A. Abdellahi and G. Ceder, *J. Electrochem. Soc.*, 2013, 160, A3179-A3197.

33.   C. M. Julien, A. Mauger and K. Zaghib, *J. Mater. Chem.*, 2011, 21, 9955-9968.

34.   A. Yamada, S. C. Chung and K. Hinokuma *J. Electrochem. Soc.*, 2001, 148, A224-A229.

35.   W.-J. Zhang, *J. Power Sources*, 2011, 196, 2962-2970.

36.   Y. Wang, P. He and H. Zhou, *Energy Environ. Sci.*, 2011, 4, 805-817.

37.   N. R. Cameron, *Polymer*, 2005, 46, 1439-1449.

38.   D. Wang, N. L. Smith and P. M. Budd, *Polym. Int.*, 2005, 54, 297-303.

39.   M. Gaberscek, R. Dominko, M. Bele, M. Remskar, D. Hanzel and J. Jamnik, *Solid State Ionics*, 2005, 176, 1801-1805.

40.   S. K. Martha, N. J. Dudney, J. O. Kiggans and J. Nanda, *J. Electrochem. Soc.*, 2012, 159, A1652-A1658.

41.   X. Zhang and T. M. Devine, *J. Electrochem. Soc.*, 2006, 153, B375-B383.

42.   K. Tang, X. Yu, J. Sun, H. Li and X. Huang, *Electrochim. Acta*, 2011, 56, 4869-4875.

43.   H. Matsui, T. Nakamura, Y. Kobayashi, M. Tabuchi and Y. Yamada, *J. Power Sources*, 2010, 195, 6879-6883.

44.   Y. Atsuo, K. Hiroshi, N. Shin-ichi, S. Noriyuki, K. Ryoji, Y. Masao, N. Tatsuya and K. Yo, *Nature Mater.*, 2006, 5, 357-360.

45.   M. Rahul, Z. Fei and G. Ceder, *Nature Mater.*, 2011, 10, 587-590.

46.   G. Pierre, C.-C. Montse, L. Lydia, L. Stephane, C. Philippe, H. Stéphane, T. Jean-Marie and M. Christian, *Nature Mater.*, 2008, 7, 741-747.

47.   P. A. Johns, M. R. Roberts, Y. Wakizaka, J. H. Sanders and J. R. Owen, *Electrochem. Commun.*, 2009, 11, 2089-2092.

48.   A. Manthiram, A. Vadivel Murugan, A. Sarkar and T. Muraliganth, *Energy Environ. Sci.*, 2008, 1, 621-638.

49.   M. R. Roberts, A. Madsen, C. Nicklin, J. Rawle, M. G. Palmer, J. R. Owen and A. L. Hector, *J. Phys.Chem. C*, 2014, 118, 6548-6557.

50.   D. Y. W. Yu, C. Fietzek, W. Weydanz, K. Donoue, T. Inoue, H. Kurokawa and S. Fujitani, *J. Electrochem. Soc.*, 2007, 154, A253-A257.

Nanoscale Accepted Manuscript

51.   J. Come, P.-L. Taberna, S. Hamelet, C. Masquelier and P. Simon, *J. Electrochem. Soc.*, 2011, 158, A1090-A1093.

52.   J. S. Newman and C. W. Tobias, *J. Electrochem. Soc.*, 1962, 109, 1183-1191.

53.   R. Amin, P. Balaya and J. Maier, *Electrochem. Solid-State Lett.*, 2007, 10, A13-A16.

54.   P. P. Prosini, M. Lisi, D. Zane and M. Pasquali, *Solid State Ionics*, 2002, 148, 45-51.

55.   A. V. Churikov, A. V. Ivanishchev, I. A. Ivanishcheva, V. O. Sycheva, N. R. Khasanova and E. V. Antipov, *Electrochim. Acta*, 2010, 55, 2939-2950.

56.   R. Malik, D. Burch, M. Bazant and G. Ceder, *Nano Lett.*, 2010, 10, 4123-4127.

57.   V. Zadin, H. Kasemägi, A. Aabloo and D. Brandell, *J. Power Sources*, 2010, 195, 6218-6224.

Nanoscale Accepted Manuscript